Supplemental Information

The pentapeptide-repeat protein, MfpA, interacts with mycobacterial DNA gyrase as a DNA T-segment mimic

Lipeng Feng[a,b], Julia E.A. Mundy[a], Clare E.M. Stevenson[a], Lesley A. Mitchenall[a], David M. Lawson[a], Kaixia Mi[b,c,*], Anthony Maxwell[a,*]

[a]Department of Biological Chemistry, John Innes Centre, Norwich Research Park, Norwich, NR4 7UH, UK;

[b]CAS Key Laboratory of Pathogenic Microbiology and Immunology, Institute of Microbiology, CAS, Beijing, 100101, China;

[c]Savaid Medical School, University of Chinese Academy of Sciences, Beijing 101408, China.

Supporting Materials and Methods

Cloning

For pACYCDuet-1-*MsgyrB-MsgyrA*, pACYCDuet-1-*MsB-A* and pACYCDuet-1-*MsB-A56* plasmids, *MsgyrA* was amplified from the *Mycobacterium smegmatis* genome and inserted into pACYCDuet-1 using NdeI and EcoRV restriction sites to obtain pACYCDuet-1-*MsgyrA*. Then *MsgyrB* was amplified from the genome and cloned into pACYCDuet-1-*MsgyrA* using EcoRI and HindIII restriction sites to obtain pACYCDuet-1-*MsgyrB-MsgyrA*. A lysine linker was introduced into the pACYCDuet-1-*MsgyrB-MsgyrA* plasmid using the Quickchange method (1) to get pACYCDuet-1-*MsB-A*. The C-terminal domain of *MsgyrA* was deleted from the pACYCDuet-1-*MsB-A* plasmid using the Quickchange method to get pACYCDuet-1-*MsB-A56*.

For the mutants of pACYCDuet-1-*MsgyrB-MsgyrA* and pACYCDuet-1-*MsB-A*, all the mutated fragments were generated using overlap-extension PCR (2) and inserted into both pACYCDuet-1-*MsgyrB-MsgyrA* and pACYCDuet-1-*MsB-A* plasmids using EcoRI and AscI restriction sites to get the mutants. For pACYCDuet-1-*MsgyrB* plasmid, the digested *MsgyrB* from the above was inserted into pACYCDuet-1 using EcoRI and HindIII restriction sites to obtain pACYCDuet-1-*MsgyrB*. For pACYCDuet-1-TEV-*MsgyrB47* plasmid, the TEV-*MsgyrB47* (427 amino acids of N-terminal of *MsgyrB*) was amplified from pACYCDuet-1-*MsgyrB* plasmid using EcoRI and HindIII restriction sites to obtain pACYCDuet-1-TEV-*MsgyrB47*. The DNA sequence for a TEV site was introduced by

the forward primer. For the mutants of pACYCDuet-1-TEV-*MsgyrB47*, all the mutated fragments were generated using overlap-extension PCR and inserted into pACYCDuet-1-TEV-*MsgyrB47* using EcoRI and HindIII restriction sites to get the mutants. For pET-28a-TEV-*MsmfpA* and pET-28a-TEV-*MsmfpB* plasmids, TEV-*MsmfpA* and TEV-*MsMfpB* were amplified from the *M. smegmatis* genome and separately inserted into pET28a using NdeI and HindIII restriction sites to obtain pET-28a-TEV-*MsmfpA* and pET-28a-TEV-*MsmfpB*. The DNA sequence of a TEV site was introduced by the forward primer. For the mutants of pET-28a-TEV-*MsmfpA*, all the mutated fragments were generated using overlap PCR and inserted into pET-28a-TEV-*MsmfpA* using NdeI and HindIII restriction sites to get the mutants. Primers used in cloning are listed in Table S1.

Protein Purification

Plasmid constructs of Msgyrase and its mutants, MsB-A and its mutants, MsB-A56, MsGyrB were transformed into *E. coli* BL21 (DE3), separately. The cultures were grown in LB with induction at OD_{600} of ~0.6-0.8 by adding 0.3 mM IPTG at 20°C for 12-16 h. The cells were harvested and resuspended in lysis buffer (20 mM Tris·HCl pH 8.0, 500 mM NaCl, 5% glycerol, 5 mM imidazole, 0.2 mM β-mercaptoethanol) and then sonicated in an ice bath. Purification of the proteins was carried out in four steps. In the first step the supernatant was applied to 6 mL Nickel-NTA beads (Qiagen). The beads were washed with lysis buffer with 30 mM imidazole. The protein was eluted with lysis buffer with 250 mM imidazole. The fractions were analyzed by 10% SDS-PAGE and dialyzed overnight against low salt buffer (50 mM Tris-HCl pH 8.0, 50 mM NaCl, 4 mM DTT). The dialyzed protein was loaded into a 5 mL Heparin column (GE) and eluted with a gradient from 50 mM to 500 mM NaCl. The fractions were analyzed by 10% SDS-PAGE and dialyzed against low-salt buffer (50 mM Tris-HCl pH 8.0, 50 mM NaCl, 4 mM DTT). The sample was loaded onto a MonoQ column (GE) and eluted with a gradient from 50 mM to 500 mM NaCl. The fractions were analyzed by 10% SDS-PAGE and concentrated to ~0.6 mL. After centrifugation, the sample was further purified using a Superdex200 size exclusion column in gel filtration buffer (50 mM Tris-HCl pH 8.0, 100 mM KCl, 10% glycerol, 5 mM DTT). The fractions were analyzed by 10% SDS-PAGE and concentrated to more than 10 mg/mL. After aliquoting and flash freezing, the protein was stored at -80°C.

For MsMfpA and its mutants and MsGyrB47 and its mutants, the plasmids were transformed into

E. coli BL21 (DE3), separately. The cultures grew in LB with induction at OD_{600} of 0.6~0.8 by adding 0.3 mM IPTG at 16°C for 20 h. After purifying with nickel-NTA beads (similar method with the purification of the enzymes), the fractions were analyzed via 10% SDS-PAGE and digested overnight at 4°C by TEV protease. The digested protein was dialyzed for 3-5 h against low salt buffer (50 mM Tris-HCl pH 8.0, 100 mM NaCl, 5% glycerol, 0.2 mM β-mercaptoethanol) and purified with nickel-NTA beads. The flow-through was collected and purified with MonoQ column (similar method with the purification of the enzymes). The sample was concentrated to 0.6 mL and purified using a Superdex75 size exclusion column in gel filtration buffer (MsMfpA and its mutants: 20 mM Tris·HCl pH 8.0, 300 mM NaCl, 10% glycerol, 2 mM DTT, MsGyrB47 and its mutants: 50 mM Tris·HCl pH 8.0, 100 mM KCl, 10% glycerol, 5 mM DTT). The fractions were analyzed via 10% SDS-PAGE and concentrated. After aliquoting and flash freezing, the protein was stored at -80°C.

For His-TEV-MsMfpB, pET-28a-TEV-*MsmfpB* was transformed into *E. coli* BL21 (DE3). The cultures grew in LB with induction at OD_{600} of 0.6~0.8 by adding 0.3 mM IPTG at 16°C for 20 h. After purifying with nickel-NTA beads, the fractions were analyzed via 10% SDS-PAGE. High concentrations of the fractions were dialyzed for 3h against buffer with 20 mM Tris-HCl pH 8.0, 100 mM NaCl, 15% glycerol, 2 mM DTT. After centrifuging, aliquoting and flash freezing, the protein was stored at -80°C.

Gyrase assays

Supercoiling, assays were carried out as described for *Mycobacterium tuberculosis* DNA gyrase (3) with minor modificiations. 500 ng of relaxed pBR322 (Inspiralis Ltd.) and appropriate amounts of Msgyrase were used in 30 μL reactions with assay buffer (50 mM HEPES·KOH (pH 7.9), 6 mM magnesium acetate, 4 mM DTT, 1 mM ATP, 100 mM potassium glutamate, 2 mM spermidine, 0.05 mg/ml albumin), tRNA (0.1 mg/mL), FQs (CFX or MFX: up to 100 μM) and appropriate amounts of MsMfpA. As controls, proteins or FQs was substituted by buffers or H_2O. After 30 min incubation at 37°C, 30 μL STEB (40% (w/v) sucrose, 100 mM Tris·HCl (pH 8.0), 10 mM EDTA, 0.5 mg/ml Bromophenol Blue) and 30 μL chloroform/isoamyl alcohol (v:v, 24:1) were added to stop the reaction. 20 μL of the aqueous phase was loaded onto 1% (w/v) agarose gels. After running overnight at 18 V,

gels were stained for 30 min with 1 μg/mL ethidium bromide in TAE (40 mM Tris, 20 mM acetic acid, 1 mM EDTA) and de-stained for 15 min in TAE and the DNA visualized with a UV transilluminator. Reactions with positive-supercoiled DNA (Inspiralis Ltd.) were carried out the same way with minor adjustments; samples were analyzed on 1% (w/v) agarose gels with 0.5 μg/mL chloroquine. Relaxation assays were carried out as described above with minor adjustments: assay buffer without ATP was used in the assay and the incubation time was increased to 1 h; negatively-supercoiled pBR322 (Inspiralis Ltd.) was used as substrate.

Cleavage assays were carried out as previously described (4) with minor adjustments. 500 ng of DNA (relaxed, negatively-supercoiled or positively-supercoiled pBR322) and 20 nM Msgyrase were used in 30 μL reactions with assay buffer (with or without ATP or ADPNP), tRNA (0.1 mg/mL), FQs (CFX: 100 μM, MFX: 40 μM) and appropriate amounts of MsMfpA. After 30 min incubation at 37°C, 3 μL of 2% (w/v) SDS and 3 μL of 1 mg/mL Proteinase K were added into the reaction for another 30 min at 37°C to release linear DNA. 30 μL STEB and 30 μL chloroform/isoamyl alcohol (v:v, 24:1) were added to stop the reaction. 20 μL of the aqueous phase was loaded onto a 1% (w/v) agarose gel with (relaxed DNA) or without (negatively supercoiled DNA and positively supercoiled DNA) 0.5 μg/mL ethidium bromide. Gels, run without ethidium bromide, were stained for 30 min with 1 μg/mL ethidium bromide in TAE and de-stained for 15 min in TAE; DNA was visualized with a UV transilluminator.

ATPase assays were carried out in 96-well microtiter plates as described (4). Appropriate amounts of enzyme were used in a 50 μL reactions with assay buffer (50 mM HEPES.KOH (pH7.9), 6 mM magnesium acetate, 4 mM DTT, 100 mM potassium glutamate), linear DNA (1.5 μg), novobiocin (100 μM), NADH, PEP, PK/LDH and appropriate amounts of MsMfpA. As controls, the proteins, linear DNA, novobiocin and NADH were substituted by buffers or H_2O; 46.7 μL samples were loaded onto 96-well plates. The reactions started after pre-reading for 10 min at 37°C and adding ATP or ADP into each well. All wells were monitored for absorbance at 340 nm for about 90 min at 37°C. Data were analyzed using the formula: ATPase activity (S^{-1}) = $\Delta A/(\varepsilon \times L \times T \times C_E)$ (S: rate per sec; ΔA: the change of absorbance at OD 340 nm; ε: extinction coefficient of NADH, 6220 M^{-1} cm^{-1}; L: the height of 50 μL sample in the well, C_E: the concentration of the enzyme, M).

Crystallization

Crystallization experiments were performed at a constant temperature of 20°C using sitting-drop vapour diffusion in MRC2 96-well crystallization plates (Swissci) with a mixture of 0.3 µL precipitant (from both commercial and in-house screens) and 0.3 µL protein solution, using either an OryxNano or an Oryx8 crystallisation robot (Douglas Instruments). A variety of commercially available and in-house screens were set up, and promising hits were subsequently optimized. For MsMfpA, the protein concentration was 4 mg/ml in buffer with 20 mM Tris·HCl pH 8.0, 100 mM NaCl, 10% (v/v) glycerol, 2 mM DTT, and the best diffracting crystals were obtained from a precipitant solution comprised of 0.1 M sodium acetate pH 4.6, 2.0 M sodium formate. For MsGyrB47, equal amounts of MsMfpA and MsGyrB47 (each of them is about 2 mg/mL) were mixed in 20 mM Tris·HCl pH 8.0, 300 mM NaCl, 2 mM DTT buffer with 1 mM ADPNP and Mg^{2+}, and the best diffracting crystals were obtained from a precipitant solution comprised of 2.1 M DL-malic acid pH 7.0. For the MsMfpA-MsGyrB47 complex, equal amounts of MsMfpA and MsGyrB47 (each of them is about 2 mg/mL) were mixed in 20 mM Tris·HCl pH 8.0, 300 mM NaCl, 2 mM DTT buffer without nucleotide, and the best diffracting crystals were obtained from a precipitant solution comprised of 0.1 M Na·HEPES pH 7.0, 0.15 M ammonium sulfate, 20% (v/v) PEG4000. Suitable crystals were cryoprotected using the crystallisation conditions supplemented with 25% (v/v) ethylene glycol then flash-cooled in liquid nitrogen using LithoLoops (Molecular Dimensions) prior to transport to the synchrotron.

Data collection, structure determination and refinement

X-ray data were recorded either on beamline I03 or I04 at the Diamond Light Source (Oxfordshire, UK) using either a Pilatus3 6M or an Eiger2 XE 16M hybrid photon counting detector (Dectris), with the crystal maintained at -173°C by a Cryojet cryocooler (Oxford Instruments). The data were integrated and scaled using DIALS (5) and then merged using AIMLESS (6); data collection statistics are summarized in Table 1.

The majority of the downstream analysis was performed through the CCP4i2 graphical-user interface (7). All structures were solved by molecular replacement using PHASER (8). For the 1.77-Å resolution MsMfpA only structure, a dimer template was prepared from the *M. tuberculosis* MfpA structure (PDB code 2BM4), with which it shares 62% sequence identity, using CHAINSAW (9); PHASER was able to locate one copy of the dimer in the asymmetric unit (ASU) of the $P2_1$ unit cell. For the 1.56-Å resolution MsGyrB47 only structure, a monomer template was prepared from the *M. tuberculosis* GyrB47 structure (PDB code 3ZKB), with which it shares 82% sequence identity, using CHAINSAW; PHASER was able to locate one copy of the subunit in the ASU of the $P6_122$ unit cell, and a recognisable dimer was formed through the application of two-fold

crystallographic symmetry. For the 2.2-Å resolution MsMfpA-MsGyrB47 complex, the previous two structures (after refinement) were used as inputs to PHASER, which located one copy of the MsMfpA dimer plus one copy of the MsGyrB47 subunit in the ASU of the *C*2 unit cell. The three structures were completed through several iterations of model building with COOT (10) and restrained refinement with REFMAC5 (11). TLS group definitions obtained from the TLSMD server (http://skuld.bmsc.washington.edu/~tlsmd/) (12) were used in the later stages of refinement for the MsMfpA only structure and for the complex, whereas for the higher resolution MsGyrB47 structure, anisotropic thermal parameters were refined. The statistics of the final models, including validation output from MolProbity (13) are shown in Table 1. All structural figures were prepared using CCP4mg (14).

Table S1. List of oligonucleotide primers

Name	Sequence	Application
PTEV-MsmfpA-NdeIF	CAGTTCGCCATATGGAGAACCTGTACTTCCAATCCATGCGTATAGGGGCAAAC	For the construction of pET-28a-TEV-*MsmfpA*
PMsmfpA-HindIIIR	TATAAGCTTCTAGCCGCCGTGGACGGCC	
PMsgyrB-EcoRIF	GGCGAATTCGATGGCTGCCCAGAAGAACAAT	For the construction of pACYCDuet-1-*MsgyrB-MsgyrA*
PMsgyrB-HindIIIR	GCGAAGCTTTTAAACATCCAGGAAGCGA	
PMsgyrA-NdeIF	CAGTTCGCCATATGATGACTGATACGACGCTG	
PMsgyrA-EcoRVR	ATCGATATCTCACGCCTCGGGTGACTC	
PTEV-MsmfpB-NdeIF	CAGTTCGCCATATGGAGAACCTGTACTTCCAATCCATGGCCTACGAGCACTCTG	For the construction of pET-28a-TEV-*MsmfpB*
PMsmfpB-HindIIIR	TATAAGCTTTCAGCCGGGCAGCGGGGTC	
P-MsB-A-F	GCTTCCTGGATGTTAAGACTGATACGACGCTGCCGCCG	For the construction of pACYCDuet-1-*MsB-A*
P-MsB-A-R	GTCGTATCAGTCTTAACATCCAGGAAGCGAACGTCTTTG	
P-MsB-A56-F	CATCGTGCCCTGAGATATCTCGCTGACGTCGGTACCCTCGAG	For the construction of pACYCDuet-1-*MsB-A56*
P-MsB-A56-R	CGTCAGCGAGATATCTCAGGGCACGATGCGGGTCCGACGC	
PTEV-	GGCGAATTCGGAGAACCTGTACTTCCAATCCA	For the

MsgyrB-EcoRIF	TGGCTGCCCAGAAGAACAAT	construction of pACYCDuet-1-TEV-*MsgyrB47*
PMsgyrB47-HindIIIR	GCGAAGCTTTCACACCAACTCACGCGCCTTACG	
PMsGyrB47-D348A-F	AACCTCACCGGTGCGGACATCCGTGAGGGTTTGGCGGCGG	For the construction of mutated pACYCDuet-1-TEV-*MsgyrB47*, pACYCDuet-1-*MsB-A* and pACYCDuet-1-*MsgyrB-MsgyrA* on interface I
PMsGyrB47-D348A-R	TCACGGATGTCCGCACCGGTGAGGTTGGGATCCTTGTC	
PMsGyrB47-R421A-HindIIIR	CGCAAGCTTTCACACCAACTCACGCGCCTTGGCCGCCGCGATCCGCGCCTGCGCC	
PMsGyrB-R421A-F	GGATCGCGGCGGCCAAGGCGCGTGAGTTGGTGCGGCGT	
PMsGyrB-R421A-R	TCACGCGCCTTGGCCGCCGCGATCCGCGCCTGCGCCGAC	
PMsGyrB-AscIR	TACGGCGCGCCTCGACGTCTTCGCCCATG	
PMsGyrB E136A-F	CGACGCGGCTGGCGGCCACGGTCCTGCGTGACGGGTAC	For the construction of mutated pACYCDuet-1-*MsB-A* and pACYCDuet-1-*MsgyrB-MsgyrA* on interface II
PMsGyrB E136A-R	AGGACCGTGGCCGCCAGCCGCGTCGACAGCGCGTTCAC	
PMsGyrB K159A-F	CCGGCAAGCTCGCGCAGGGCGGTGAGACCAAGGAGACC	
PMsGyrB K159A-R	TCACCGCCCTGCGCGAGCTTGCCGGGCACCGAGCGGTC	
PMsMfpA-R116A-F	TGTCGGACTGCGCGTTGCGTGAGGTCTCGCTCGTCGGTG	For the construction of mutated pET-28a-TEV-*MsmfpA* on interface I
PMsMfpA-R116A-R	ACCTCACGCAACGCGCAGTCCGACAGGTCGACGGCACGC	
PMsMfpA-E119Q-F	GCCGGTTGCGTCAGGTCTCGCTCGTCGGTGCGGATCTGC	
PMsMfpA-E119Q-R	ACGAGCGAGACCTGACGCAACCGGCAGTCCGACAGGTCG	
PMsMfpA-R116AE119Q-F	GGACTGCGCGTTGCGTCAGGTCTCGCTCGTCGGTGCGGATCTGC	
PMsMfpA-R116AE119Q-R	GCGAGACCTGACGCAACGCGCAGTCCGACAGGTCGACGGCACGC	
PMsMfpA-	ATTTCAGCGGCGTCAACCTCTCGGAGTCCGA	For the

D46N-F	GCATCATGGAT	construction of mutated pET-28a-TEV-*MsmfpA* on interface II
PMsMfpA-D46N-R	TCCGAGAGGTTGACGCCGCTGAAATCGCATTCGGTGAACACGACG	
PMsMfpA R64A-F	GCACGTTCCGCGCGAGCACCATCTGGCACAGCACGTTC	
PMsMfpA R64A-R	CAGATGGTGCTCGCGCGGAACGTGCAGTTGCGGAACGC	

Figure legends

Figure S1. The activities of Ms gyrase at a range of enzyme concentrations. (A) supercoiling, (B) the conversion of positively supercoiled DNA to negatively supercoiled DNA and (C) relaxation. (D) Relaxation assays with negatively-supercoiled DNA were performed using increasing concentrations of MsMfpA. The actions of MsMfpA on Msgyrase activity with positively supercoiled DNA as substrate were determined with 100 μM CFX (E) or MFX (F) in the presence of ATP. (G) Supercoiling assay with MsMfpA and increasing concentrations of MsMfpB in the presence of 100 μM CFX and 1 mM GTP. G: Msgyrase.

Figure S2. DNA cleavage assays with Ms gyrase. (A) Cleavage assay with MsMfpA and increasing concentration of MsMfpB in the presence of 100 μM CFX and 1 mM GTP. (B) Cleavage assays were performed using positively-supercoiled DNA as substrate with 100 μM CFX or 40 μM MFX in the presence of ATP. The inhibitory effects of MsMfpA on CFX- (B and D) or MFX- (C and E) induced cleavage were determined using negatively (B and C) or positively (D and E) supercoiled DNA in the absence or presence of ATP.

Figure S3. Activities of MsB-A and MsB-A56. (A) The supercoiling activity of MsB-A was determined using different concentrations of enzyme. The effects on CFX- or MFX-induced cleavage by MsB-A (B) or MsB-A56 (C) by MsMfpA in the presence of ATP. (D) ATPase assays were performed with linear DNA, different concentrations of MsMfpA or both.

Figure S4. (A) The crystal structure of the MsMfpA homodimer determined at 1.77 Å resolution; the biologically relevant assembly is shown, and this corresponds to the asymmetric unit (ASU). (B) The crystal structure of the MsMfpA-MsGyrB47 2:1 complex determined at 2.20 Å resolution. Shown is the ASU with the presumed biologically relevant interaction between the partner proteins via interface

I. Further work is needed to establish whether this corresponds to the full biologically relevant assembly. (C) Superposition of MsGyrB47 homodimer (from panel D; shown semi-transparent) onto the MsMfpA-MsGyrB47 2:1 complex (from panel B) based on the yellow MsGyrB47 subunits only (yellow subunit not shown for the complex). This is equivalent to the superposition shown in panel E, but viewed from different direction. (D) The crystal structure of the MsGyrB47 homodimer in complex with ADPNP determined at 1.56 Å resolution. In this crystal form, the ASU corresponds to a single subunit and the biologically relevant homodimer is generated through the application of two-fold crystallographic symmetry. (E) Superposition of MsMfpA-MsGyrB47 2:1 complex (from panel B; shown semi-transparent) onto the MsGyrB47 homodimer (from panel D) based on the yellow MsGyrB47 subunits only (yellow subunit not shown for the complex). This is equivalent to the superposition shown in panel C, but viewed from different direction. (F) Crystal structure of the ATPase domain of topoisomerase IV from *Streptococcus pneumoniae* in complex with ADPNP and T segment DNA (15). In this view, the long axis of the DNA fragment is perpendicular to the plane of the image. It is clear from panels C and E that the relationship between the components of the 2:1 complex is incompatible with the formation of a MsGyrB47 homodimer akin to that seen in panel D, since there would be major steric clashes between the green MsGyrB47 subunit and the blue MsMfpA subunit. Moreover, from a comparison of panels E and F, it can be seen that the orientation of the MsMfpA homodimer with respect to the yellow MsGyrB47 is essentially orthogonal to the orientation of the T segment DNA with respect to the yellow topoisomerase IV subunit.

In all panels, the protein is depicted in cartoon representation with different colors to distinguish the individual subunits, and with the bound nucleotides (where present) displayed as van der Waals spheres. Panels A-C are shown in the same orientation with respect to the MsMfpA homodimer. Panels D-F are shown in the same orientation with respect to the MsGyrB47 homodimer

Figure S5. A comparison of the structures of MsGyrB47 seen in the homodimer and in the 2:1 complex with MfpA reveals a hinge-bending movement and the reorientation of a loop bearing two key residues. A superposition based on the N-terminal ATPase subdomain shows that the C-terminal transducer subdomain rotates by ~20° as a result of subtle changes in the backbone torsion angles in the connecting loop between the two subdomains (residues 252-256), which is referred to as the "hinge" and illustrated in the overview image (left). In the close-up on the right, several residues

implicated in ATP binding and hydrolysis in the MsGyrB47 homodimer are shown in stick representation (with pale yellow carbons, except for Tyr12 from the opposing subunit, where the carbons are pale green). Sections of the associated main-chain are also shown in cartoon representation (with the same color scheme). In this overlay, in MsGyrB47 from the 2:1 complex (pink), only Glu48 and Asn52 have any structural correspondence: Tyr12 is not present because MsGyrB47 is monomeric in this structure, Lys108 is disordered, and the "QK loop" bearing Glu370 and Lys373 is displaced, in part due to the interdomain hinge bending, and in part due to the reorientation of this loop. Thus, the conformation and stoichiometry of MsGyrB47 in the 2:1 complex are unlikely to support nucleotide binding.

Figure S6. Schematic showing the procedure used to generate a model of a hypothetical MsMfpA-MsGyrB47 2:2 complex using a combination of elements taken from the crystal structures of the MsGyrB47-ADPNP homodimer (1) and the MsMfpA-MsGyrB47 2:1 complex (2). These elements (4 and 5) were treated as rigid bodies and could be juxtaposed in COOT such that the break points between the subdomains were in close proximity. These break points were then resealed by real space regularization of the local geometry. The resultant model is shown in Figure S7. The lower panel shows a comparison of the MsGyrB47 conformations seen in the two crystal structures and the 2:2 model (1, 2 and 6, respectively). The conformation in the latter approximates to an extrapolation of the hinge bending motion observed crystallographically, although the trajectory is slightly different, such that the angle of rotation between 1 and 6 is smaller than the sum of the angles between 1 and 2 and between 2 and 6.

Figure S7. Orthogonal views of the hypothetical MsMfpA-MsGyrB47 2:2 complex created using the procedure outlined in Figure S6. Individual subunits are shown in different colors (MsGyrB47: yellow and green; MsMfpA: blue and pink). The ADPNP retained from the MsGyrB47 homodimer structure is shown as van der Waals spheres, but the extreme rotation of the two domains with respect to one another would place the QK loop (which binds to the γ-phosphate in the crystal structure; see Figure S5) a long way from the active site. Thus, such a structure could be incapable of binding ATP.

Figure S8. Activities of Ms gyrase mutants. (A) The rate of hydrolysis of ATP was determined using

MsGyrB47 and its mutants (mutations on interface I) with increasing concentration of wild-type MsMfpA. (B) The supercoiling activities of MsB-A and its mutants (mutations on interface I) were examined. (C) The supercoiling activities of Msgyrase and its mutants (mutations on interface I) were examined. WT: Wildtype MsB-A (B) or Msgyrase (C), D348A: MsB-A D348A (B) or Msgyrase D348A (C), R421A: MsB-A R421A (B) or Msgyrase R421A (C), D348AR421A: MsB-A D348AR421A (B) or Msgyrase D348AR421A (C). (D) The protective effects on Msgyrase, Msgyrase (D348A), Msgyrase (R421A) and Msgyrase (D348A, R421A) by MsMfpA against 100 μM CFX in time-course supercoiling assays. (E) The protective effects on Msgyrase (left) Msgyrase mutants (right) by MsMfpA mutants against 100 μM MFX in time-course supercoiling assays.

Figure S9. The protection on Msgyrase (left) Msgyrase mutants (right) by MsMfpA mutants (mutations on interface I) against 100 μM MFX in time-course supercoiling assays.

Supplementary References

1. H. Liu, J. H. Naismith, An efficient one-step site-directed deletion, insertion, single and multiple-site plasmid mutagenesis protocol. *BMC biotechnology* **8**, 91 (2008).
2. R. Higuchi, B. Krummel, R. K. Saiki, A general method of in vitro preparation and specific mutagenesis of DNA fragments: study of protein and DNA interactions. *Nucleic Acids Res* **16**, 7351-7367 (1988).
3. S. Karkare, F. Yousafzai, L. A. Mitchenall, A. Maxwell, The role of Ca(2)(+) in the activity of Mycobacterium tuberculosis DNA gyrase. *Nucleic Acids Res* **40**, 9774-9787 (2012).
4. S. Karkare *et al.*, The naphthoquinone diospyrin is an inhibitor of DNA gyrase with a novel mechanism of action. *J Biol Chem* **288**, 5149-5156 (2013).
5. G. Winter *et al.*, DIALS: implementation and evaluation of a new integration package. *Acta Crystallogr D Struct Biol* **74**, 85-97 (2018).
6. P. R. Evans, G. N. Murshudov, How good are my data and what is the resolution? *Acta Crystallogr D Biol Crystallogr* **69**, 1204-1214 (2013).
7. L. Potterton *et al.*, CCP4i2: the new graphical user interface to the CCP4 program suite. *Acta Crystallogr D Struct Biol* **74**, 68-84 (2018).
8. A. J. McCoy *et al.*, Phaser crystallographic software. *J. Appl. Crystallogr.* **40**, 658-674 (2007).
9. N. Stein, CHAINSAW: a program for mutating pdb files used as templates in molecular replacement. *J Appl Crystallogr* **41**, 641-643 (2008).
10. P. Emsley, K. Cowtan, Coot: model-building tools for molecular graphics. *Acta Cryst.* **D60**, 2126-2132 (2004).
11. G. N. Murshudov *et al.*, REFMAC5 for the refinement of macromolecular crystal structures. *Acta Crystallogr D Biol Crystallogr* **67**, 355-367 (2011).
12. J. Painter, E. A. Merritt, Optimal description of a protein structure in terms of multiple groups undergoing TLS motion. *Acta Cryst.* **D62**, 439-450 (2006).

13. I. W. Davis *et al.*, MolProbity: all-atom contacts and structure validation for proteins and nucleic acids. *Nucleic Acids Res* **35**, W375-383 (2007).
14. S. McNicholas, E. Potterton, K. S. Wilson, M. E. Noble, Presenting your structures: the CCP4mg molecular-graphics software. *Acta Crystallogr D Biol Crystallogr* **67**, 386-394 (2011).
15. I. Laponogov *et al.*, Trapping of the transport-segment DNA by the ATPase domains of a type II topoisomerase. *Nature communications* **9**, 2579 (2018).

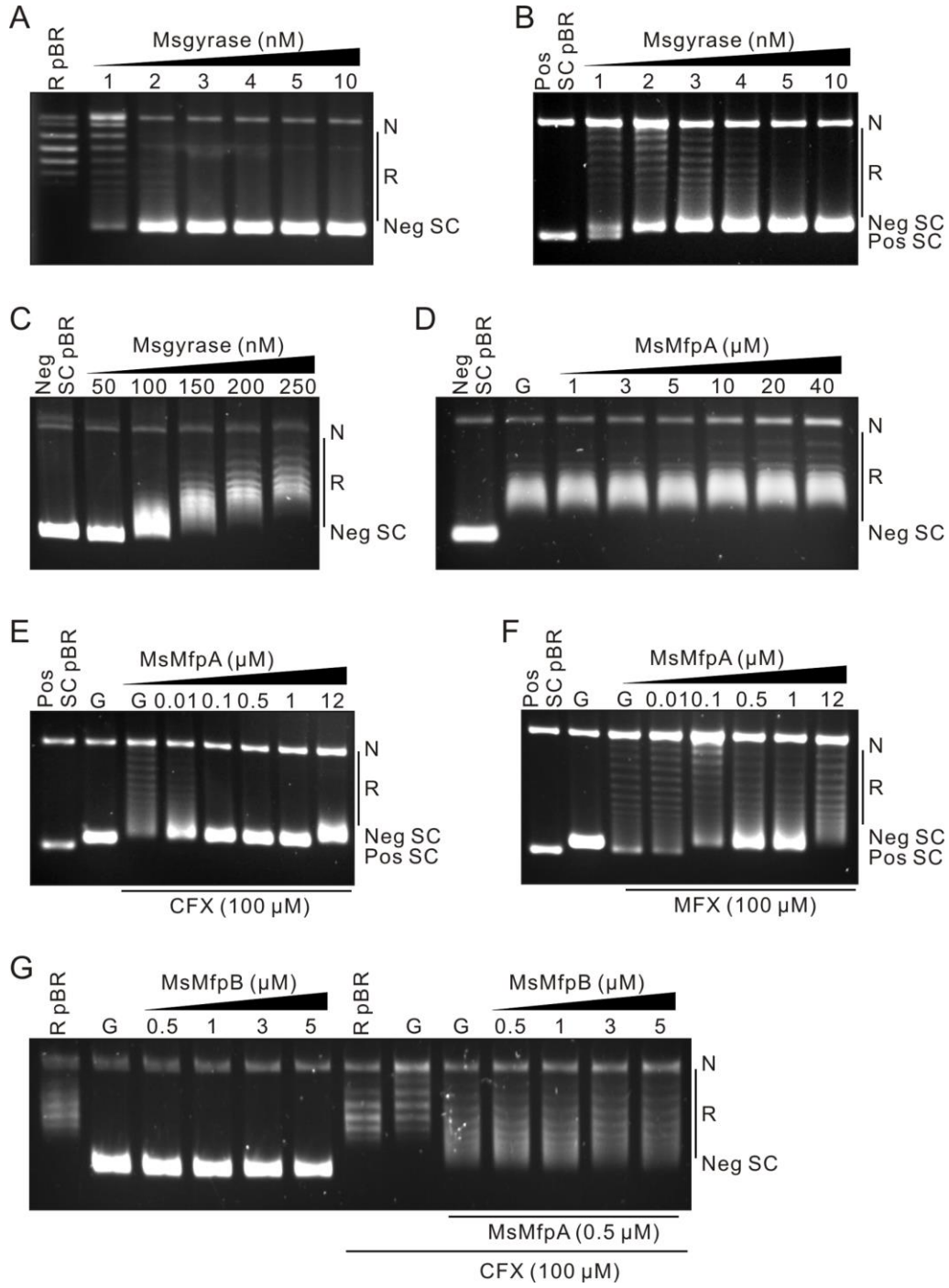
A
R pBR
Msgyrase (nM)
1 2 3 4 5 10
N
R
Neg SC
B
Pos SC pBR
Msgyrase (nM)
1 2 3 4 5 10
N
R
Neg SC
Pos SC
C
Neg SC pBR
Msgyrase (nM)
50 100 150 200 250
N
R
Neg SC
D
Neg SC pBR
MsMfpA (μM)
G 1 3 5 10 20 40
N
R
Neg SC
E
Pos SC pBR
MsMfpA (μM)
G G 0.01 0.1 0.5 1 12
N
R
Neg SC
Pos SC
CFX (100 μM)
F
Pos SC pBR
MsMfpA (μM)
G G 0.01 0.1 0.5 1 12
N
R
Neg SC
Pos SC
MFX (100 μM)
G
R pBR
MsMfpB (μM)
G 0.5 1 3 5
R pBR
MsMfpB (μM)
G G 0.5 1 3 5
N
R
Neg SC
MsMfpA (0.5 μM)
CFX (100 μM)

Fig. S1

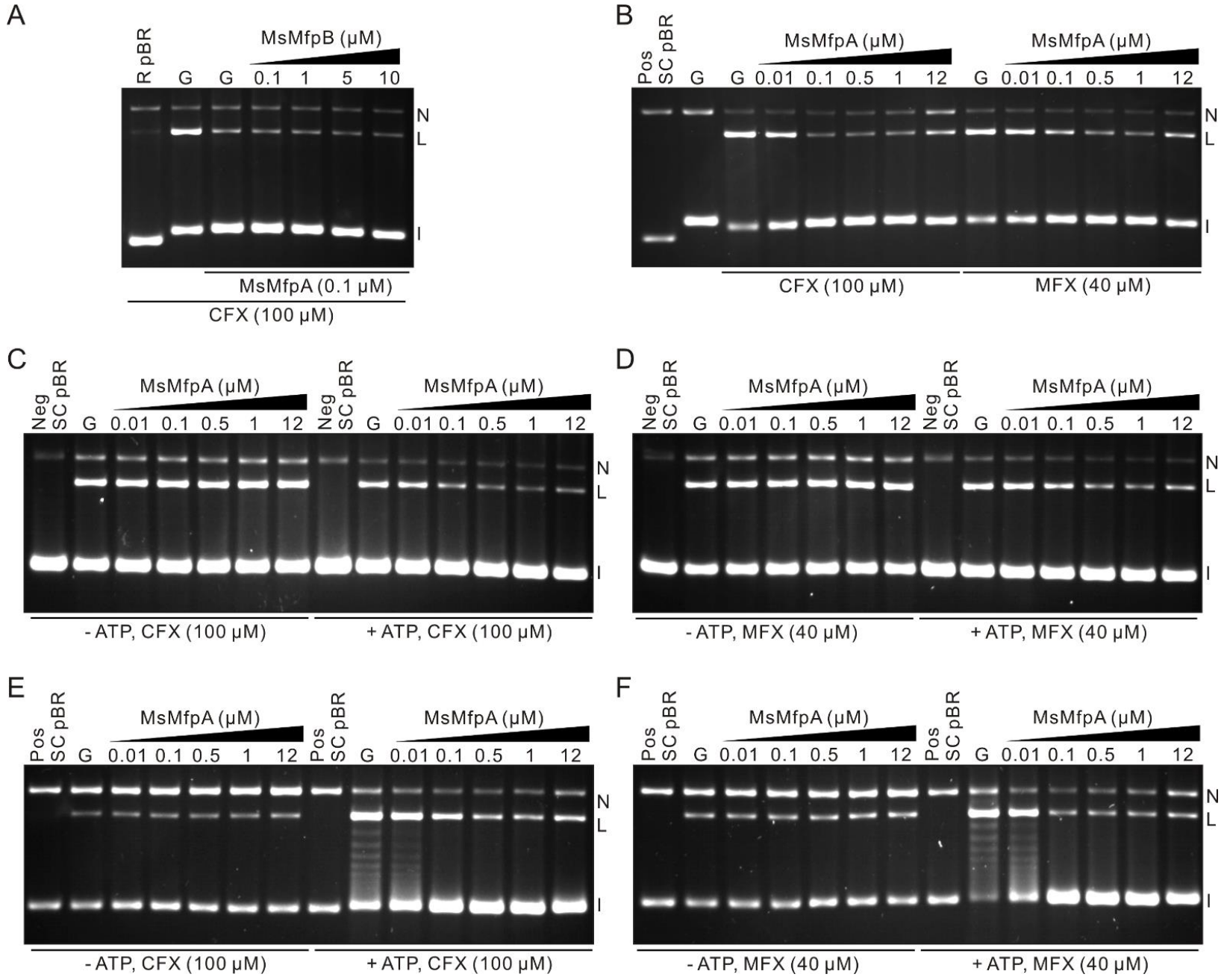
A
R pBR
G
G
MsMfpB (μM)
0.1
1
5
10
N
L
I
MsMfpA (0.1 μM)
CFX (100 μM)
B
Pos
SC pBR
G
G
MsMfpA (μM)
0.01
0.1
0.5
1
12
G
MsMfpA (μM)
0.01
0.1
0.5
1
12
N
L
I
CFX (100 μM)
MFX (40 μM)
C
Neg
SC pBR
G
MsMfpA (μM)
0.01
0.1
0.5
1
12
Neg
SC pBR
G
MsMfpA (μM)
0.01
0.1
0.5
1
12
N
L
I
- ATP, CFX (100 μM)
+ ATP, CFX (100 μM)
D
Neg
SC pBR
G
MsMfpA (μM)
0.01
0.1
0.5
1
12
Neg
SC pBR
G
MsMfpA (μM)
0.01
0.1
0.5
1
12
N
L
I
- ATP, MFX (40 μM)
+ ATP, MFX (40 μM)
E
Pos
SC pBR
G
MsMfpA (μM)
0.01
0.1
0.5
1
12
Pos
SC pBR
G
MsMfpA (μM)
0.01
0.1
0.5
1
12
N
L
I
- ATP, CFX (100 μM)
+ ATP, CFX (100 μM)
F
Pos
SC pBR
G
MsMfpA (μM)
0.01
0.1
0.5
1
12
Pos
SC pBR
G
MsMfpA (μM)
0.01
0.1
0.5
1
12
N
L
I
- ATP, MFX (40 μM)
+ ATP, MFX (40 μM)

Fig. S2

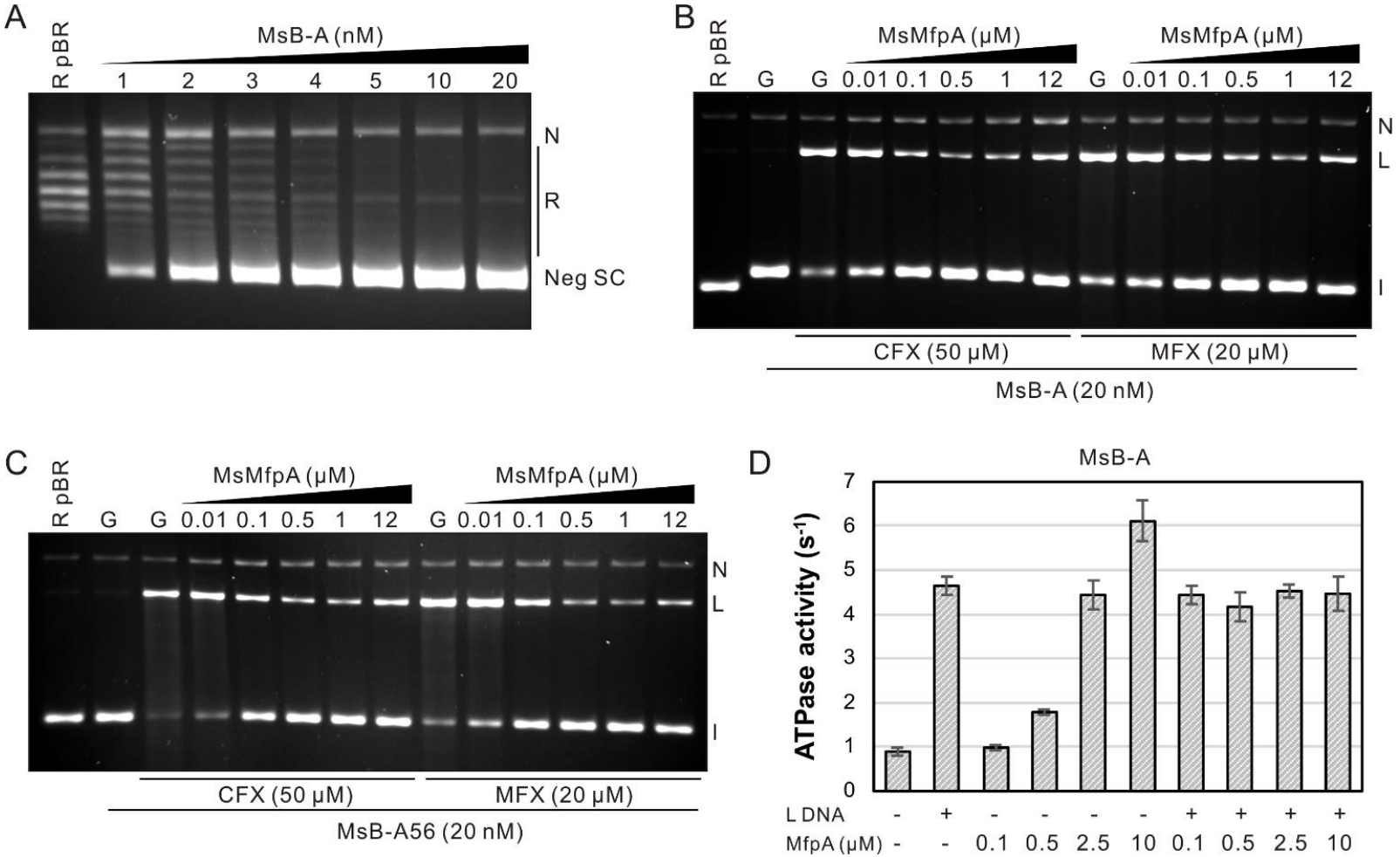
A
R pBR
MsB-A (nM)
1 2 3 4 5 10 20
N
R
Neg SC
B
R pBR
G G 0.01 0.1 0.5 1 12 G 0.01 0.1 0.5 1 12
MsMfpA (μM)
MsMfpA (μM)
N
L
I
CFX (50 μM)
MFX (20 μM)
MsB-A (20 nM)
C
R pBR
G G 0.01 0.1 0.5 1 12 G 0.01 0.1 0.5 1 12
MsMfpA (μM)
MsMfpA (μM)
N
L
I
CFX (50 μM)
MFX (20 μM)
MsB-A56 (20 nM)
D
MsB-A
ATPase activity (s-1)
0 1 2 3 4 5 6 7
L DNA - + - - - - + + + +
MfpA (μM) - - 0.1 0.5 2.5 10 0.1 0.5 2.5 10

Fig. S3

A

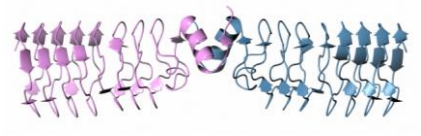

MfpA homodimer (1.77-Å resolution crystal structure)

B

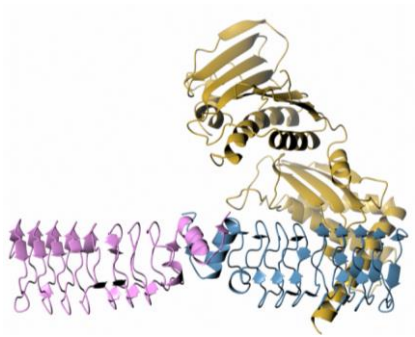

MfpA-GyrB47 2:1 complex (2.20-Å resolution crystal structure)

C

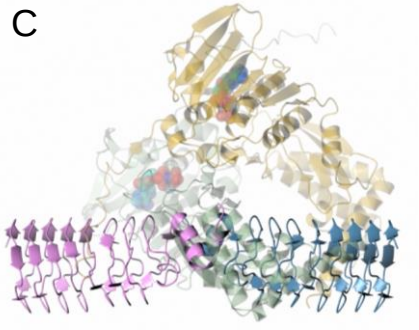

Superposition of D (semi-transparent) onto B based on yellow subunits only (yellow subunit not shown for B). Equivalent to E, but viewed from different direction.

D

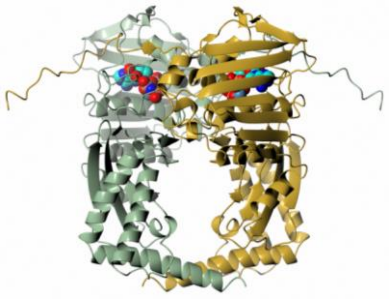

GyrB47 homodimer with ADPNP (1.56-Å resolution crystal structure)

E

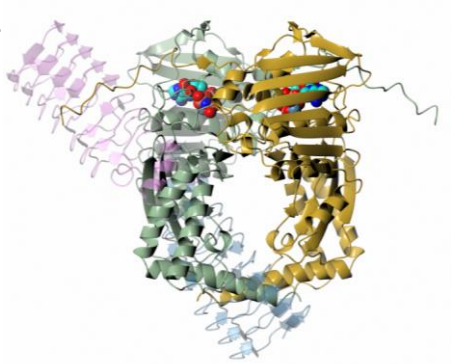

Superposition of B (semi-transparent) onto D based on yellow subunits only (yellow subunit not shown for B). Equivalent to C, but viewed from different direction.

F

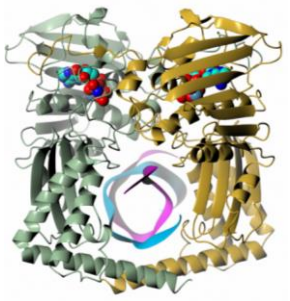

S. pneumoniae Topo IV ATPase homodimer in complex with T segment DNA (from 5J5Q)

Fig. S4

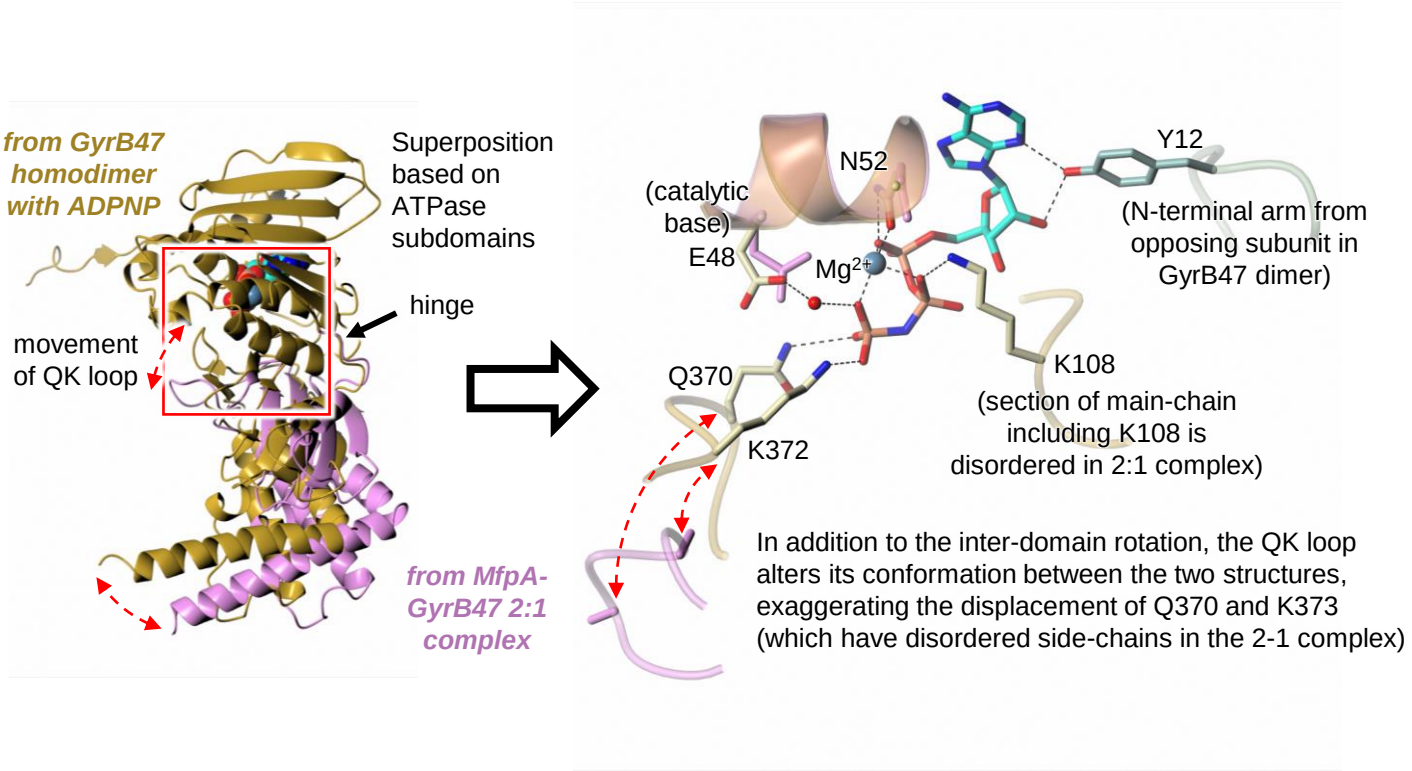
from GyrB47 homodimer with ADPNP
Superposition based on ATPase subdomains
hinge
movement of QK loop
from MfpA-GyrB47 2:1 complex
N52
(catalytic base)
E48
Mg2+
Y12
(N-terminal arm from opposing subunit in GyrB47 dimer)
Q370
K372
K108
(section of main-chain including K108 is disordered in 2:1 complex)
In addition to the inter-domain rotation, the QK loop alters its conformation between the two structures, exaggerating the displacement of Q370 and K373 (which have disordered side-chains in the 2-1 complex)

Fig. S5

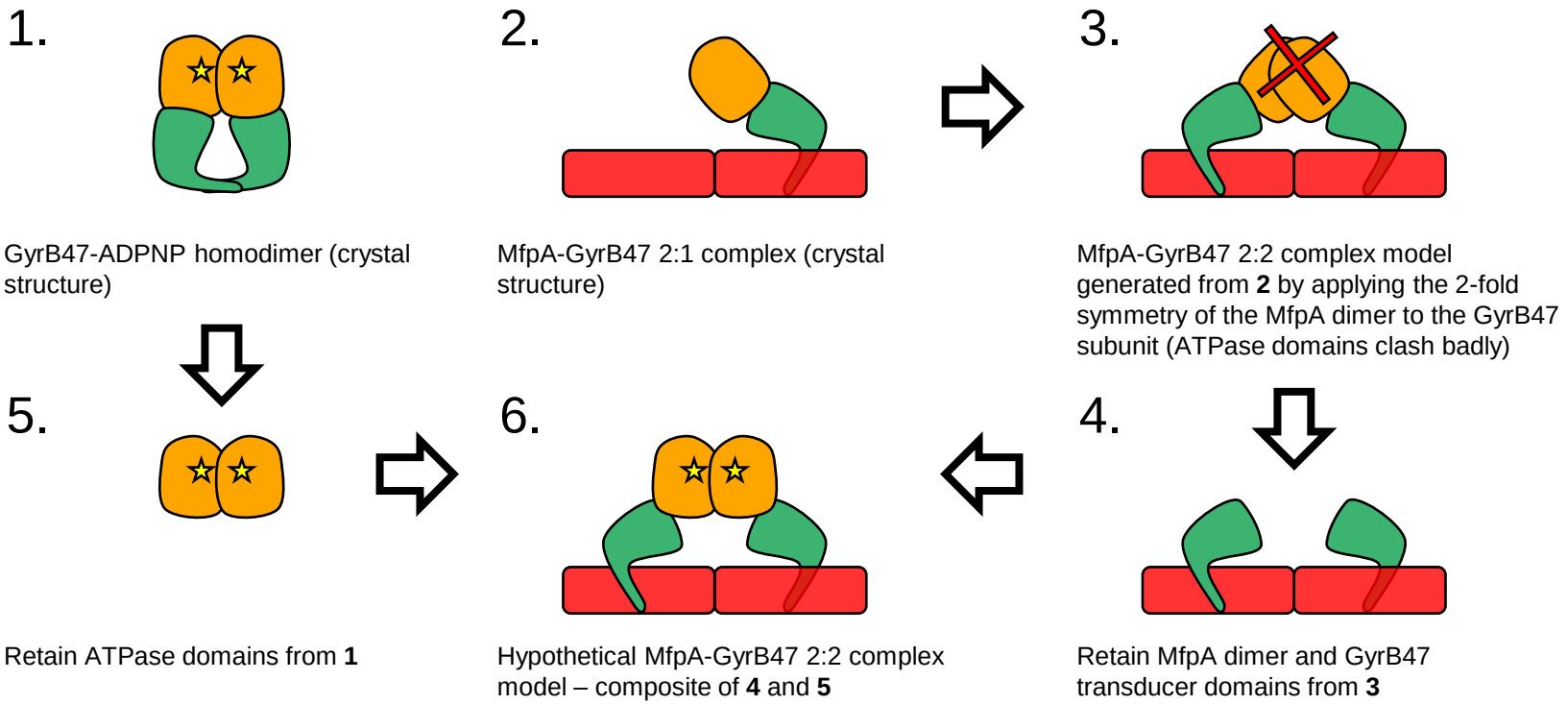

Comparison of GyrB47 conformations

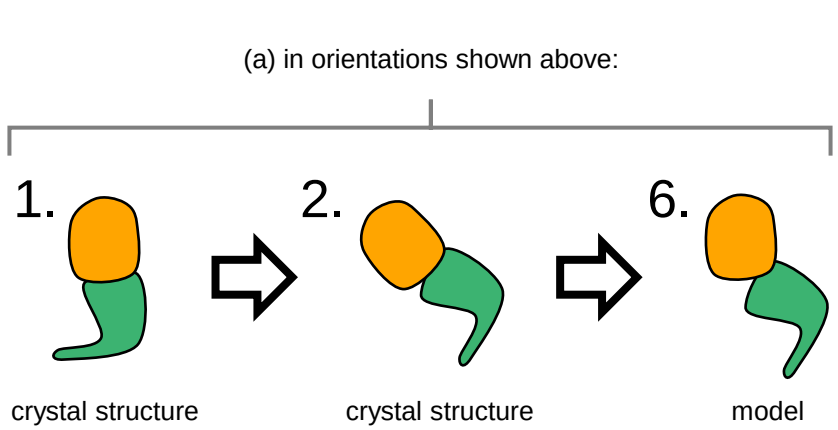

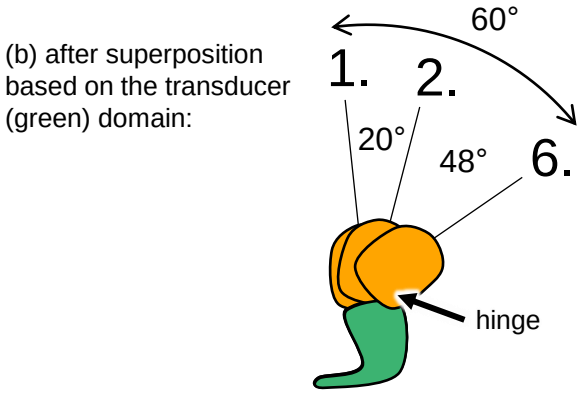

Fig. S6

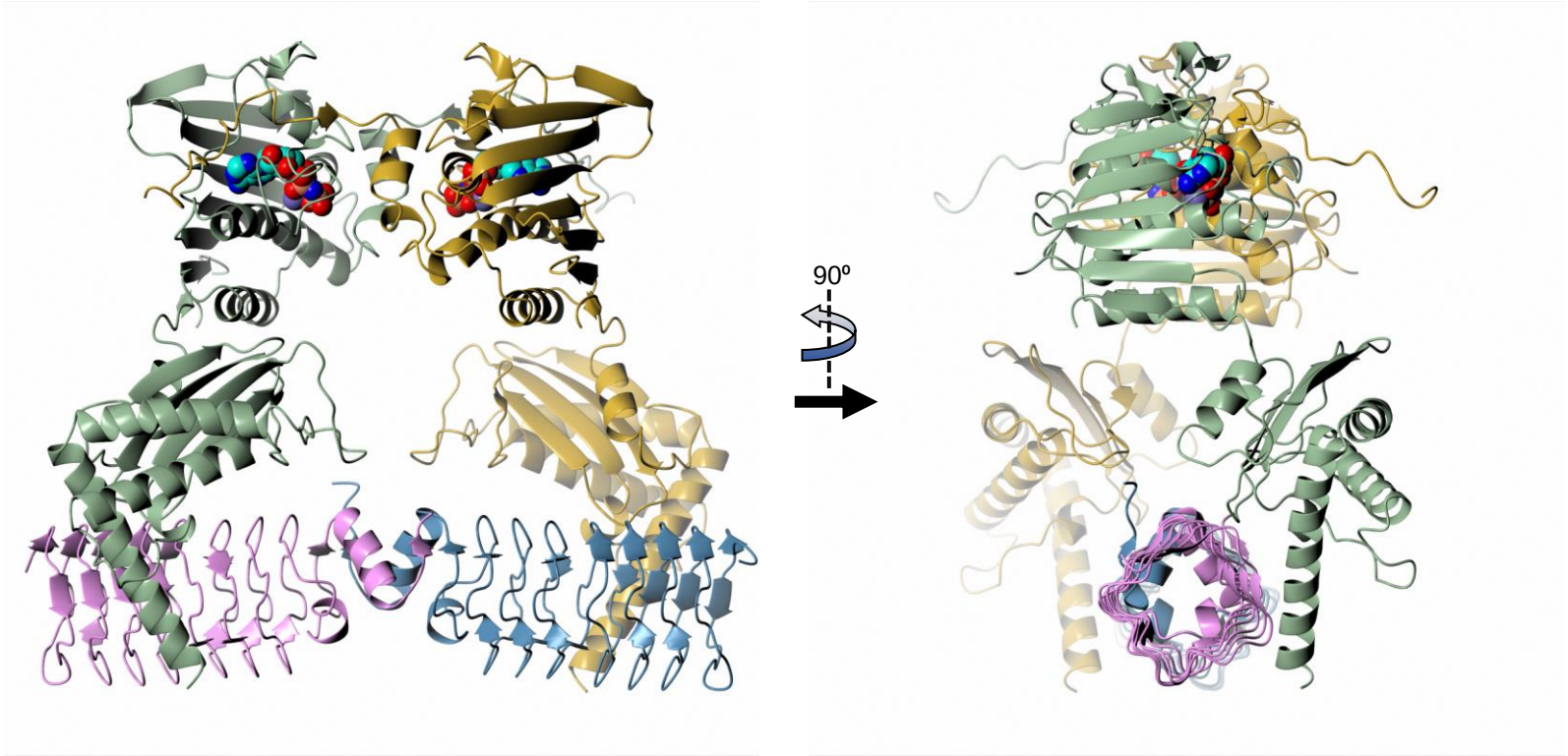

Fig. S7

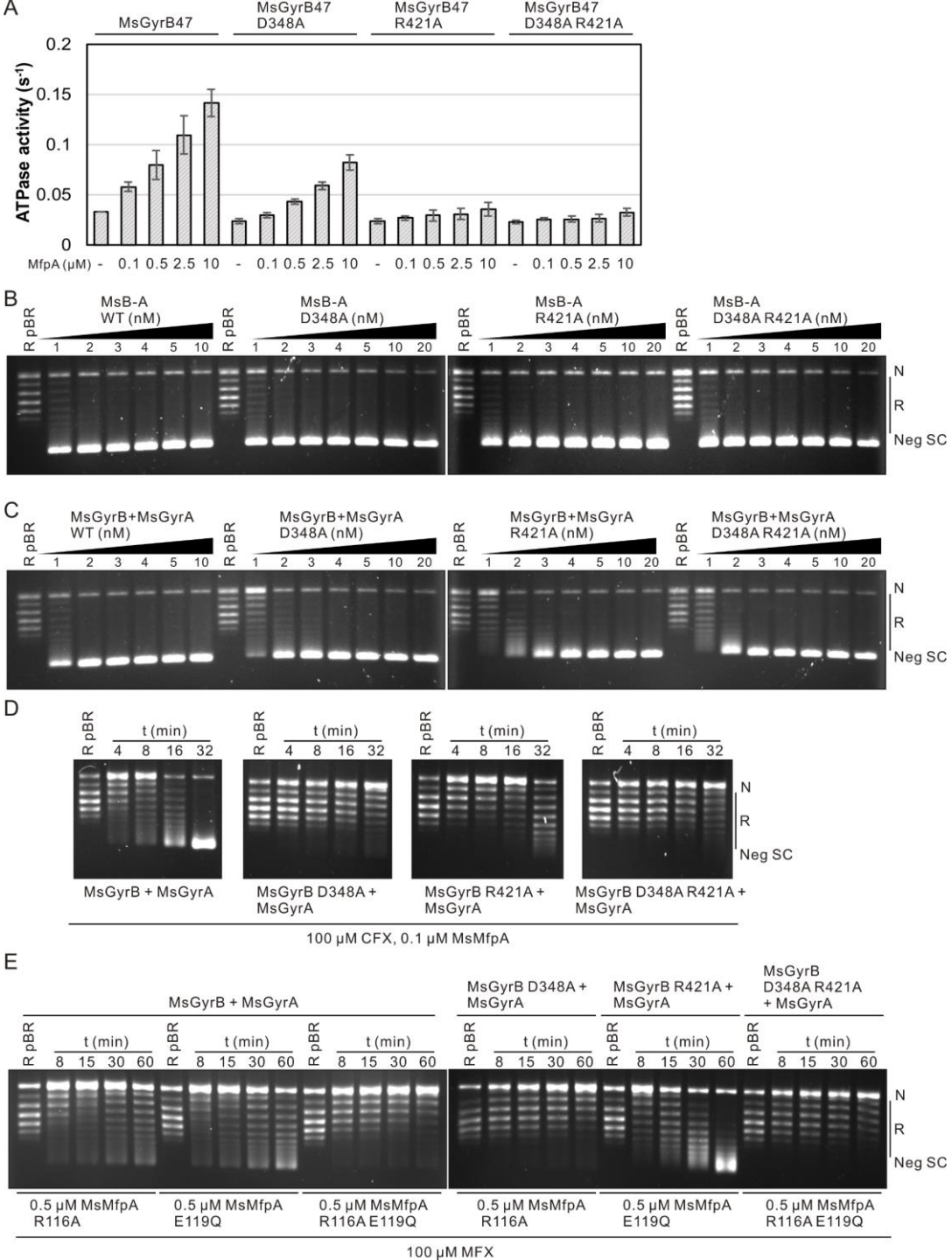
A
MsGyrB47
MsGyrB47 D348A
MsGyrB47 R421A
MsGyrB47 D348A R421A
ATPase activity (s-1)
0.2
0.15
0.1
0.05
0
MfpA (μM) - 0.1 0.5 2.5 10 - 0.1 0.5 2.5 10 - 0.1 0.5 2.5 10 - 0.1 0.5 2.5 10
B
R pBR
MsB-A WT (nM)
1 2 3 4 5 10
MsB-A D348A (nM)
1 2 3 4 5 10 20
MsB-A R421A (nM)
MsB-A D348A R421A (nM)
N
R
Neg SC
C
MsGyrB+MsGyrA WT (nM)
MsGyrB+MsGyrA D348A (nM)
MsGyrB+MsGyrA R421A (nM)
MsGyrB+MsGyrA D348A R421A (nM)
D
t (min)
4 8 16 32
MsGyrB + MsGyrA
MsGyrB D348A + MsGyrA
MsGyrB R421A + MsGyrA
MsGyrB D348A R421A + MsGyrA
100 μM CFX, 0.1 μM MsMfpA
E
MsGyrB + MsGyrA
MsGyrB D348A + MsGyrA
MsGyrB R421A + MsGyrA
MsGyrB D348A R421A + MsGyrA
8 15 30 60
0.5 μM MsMfpA R116A
0.5 μM MsMfpA E119Q
0.5 μM MsMfpA R116A E119Q
100 μM MFX

Fig. S8

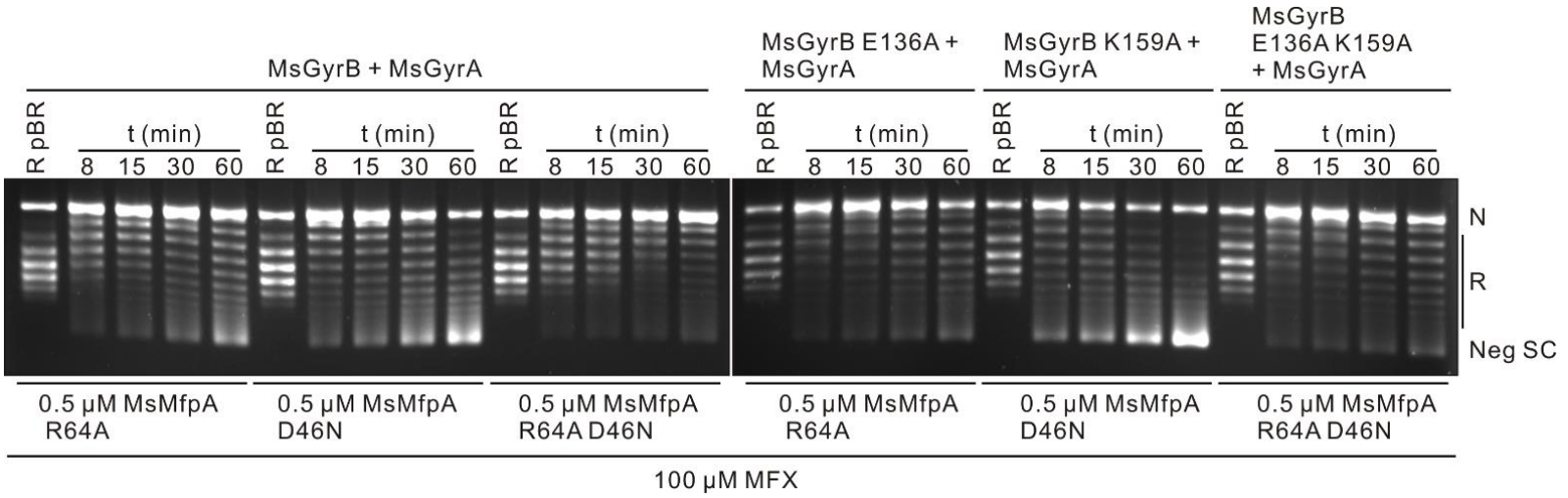
MsGyrB + MsGyrA
MsGyrB E136A + MsGyrA
MsGyrB K159A + MsGyrA
MsGyrB E136A K159A + MsGyrA
R pBR
t (min)
8 15 30 60
N
R
Neg SC
0.5 μM MsMfpA R64A
0.5 μM MsMfpA D46N
0.5 μM MsMfpA R64A D46N
100 μM MFX

Fig. S9